Development, Validation, and Application of a Parametric Finite Element Femur Model

K.F. Klein[1], J.D. Rupp[1], and J. Hu[1]
[1]University of Michigan

ABSTRACT

Older, obese, and female occupants have higher risk of serious lower-extremity injuries in frontal crashes. Optimizing vehicle restraints to better protect of these vulnerable populations, requires finite element (FE) models of the human body that consider the variations in skeletal geometry, body size, body shape, posture, and material properties among the population. This paper describes the development, validation, and application of a parametric femur FE model as an example of these methods for an entire lower-extremity FE model. Bone geometries were extracted from CT scans from 98 subjects. A landmark-based mesh morphing and projecting process was used to fit a template mesh to the femur geometry from each subject. Thicknesses of cortical bone at each node of the template mesh were programmatically determined. The nodal coordinates and the cortical bone thicknesses of the fitted meshes were analyzed using principal component analysis and regression analysis to develop a statistical model of the femur that predicts femur nodal coordinate locations representing the bone surface geometry as well as the associated cortical thickness as functions of age, BMI, and femur length. The parametric FE model was validated by running 13 subject-specific simulations and comparing measured results from a study of femur PMHS tests in combined 3-point bending and compression loading conditions to predicted results. The validated FE model was then used to investigate the effects of occupant characteristics on femur response values. The statistical model showed good fit to PMHS femur geometries, and the FE model was able to match the subject-specific test results. The average error in the force curve results for the combined loading tests was about 1%. In the initial application loading condition, an increase in BMI caused an increase in peak force, while an increase in age caused a small decrease in peak force.

INTRODUCTION

The lower extremities are now the most frequently injured body region in frontal crashes (Moran, 2003). Lower-extremity (LX) injuries account for 36% of all moderate and higher threat-to-life (Abbreviated Injury Scale 2+) injuries sustained by front-seat occupants, with about half of these LX injuries occurring in the knee-thigh-hip (KTH) complex (Kuppa and Fessahaie, 2003). Analyses of real-world crash/injury data indicate that occupant gender, age, and Body Mass Index (BMI) affect the risks of clinically significant LX injuries such that women, older occupants, and occupants with higher BMI are at increased risk of injury in frontal crashes (Moran, 2003; Rupp and Flannagan, 2011; Ridella, 2011).

2014 Ohio State University Injury Biomechanics Symposium
This paper has not been peer-reviewed.

Simulations with finite element (FE) human-body models are the most efficient method for exploring and understanding the biomechanical reasons for the effects of occupant characteristics on LX injuries and for optimizing vehicle restraints to better protect vulnerable populations. Many FE whole-body human models have been described in the literature, such as the most recent HUMOS, THUMS, and GHBMC models (Robin, 2001; Iwamoto, 2002; Torigian, 2011). Most of these models only represent an occupant who is midsize in stature and mass or the same size as adult crash test dummies (i.e. the midsize male, small female, and large male) (Hu, 2012). Many LX models and almost all KTH FE models are developed using only the geometry of the 50th percentile male (van Rooij, 2004; Kim, 2005; Ruan, 2008; and Silvestri and Ray, 2009).

Traditional methods for developing human FE models for a size different from the 50th percentile male subject include scaling existing FE models to desired sizes or developing new models based on specific subjects with the correct size (Kimpara, 2005). The scaling method is limited in that variations in external body surface geometry and bone surface geometry cannot be taken into account with simple scaling methods. The use of specific subjects to develop different sizes and shapes of human FE models is limited in that the process for this is time-consuming and costly. In addition, finding enough subjects to represent all of the size and shape variability in the population is unfeasible.

FE models of body regions that have geometry parametric with occupant characteristics have been developed for the ribcage and pediatric head. Gayzik et al. (2008) developed a statistical model that characterizes age-related changes in human rib shape, linked this model to a template FE model, and then performed simulations to explore the effect of age on thoracic response. Shi et al. (2014) developed a whole-body FE model with external surface geometry and ribcage skeletal geometry that could be varied with BMI based on the predictions of statistical geometry models and used this to explore how obesity affects occupant responses in frontal crashes. Li et al. (2011) developed a statistical model to characterize the effects of cranium geometry and material properties on pediatric head impact response for use in development of a pediatric head FE model.

No previous studies have developed entire parametric FE models of the lower extremities, although such models would be useful for understanding the biomechanical factors that explain how age, gender, and BMI affect the likelihood, location, and severity of LX injuries in frontal crashes. In this study, a parametric FE model of the femur is developed as a first step in developing and validating a parametric LX FE model. Objectives of this study are to (1) develop parametric femur FE models for males and females that have geometry parametric with occupant age, femur length (as a function of stature), and BMI; (2) validate the femur models with individual specimen responses from studies of PMHS femur tests; and (3) apply the parametric femur model to characterize the relative effects of femur length, BMI, and age for men and women on femur impact responses.

METHODS

Femur Model Development

Geometry Extraction. Clinical CT scans of male and female lower extremities were obtained from the University of Michigan Department of Radiology through a protocol approved by an institutional review board at the University of Michigan. Patients were approximately equally distributed over both genders with ages of 18-89 years, statures of 1.5-2.0 meters, and BMIs of 16-46 kg/m^2. Ninety-eight right femurs were segmented from the LX scans, and 3D surfaces were extracted using OsiriX (Pixmeo, Switzerland). 3D volume rendering mode was used for surface extraction with a Hounsfield Unit threshold value of 300, which is the default value for bone and was found to extract all bone surfaces. Coordinates of 13 anatomic landmarks, such as the most lateral point on the greater trochanter, were digitized in Rhinoceros 3D (Robert McNeel & Associates, Seattle, WA). The locations of an additional 46 landmarks were calculated based on locations of anatomic landmarks.

Morphing and Projecting Processes. The first step in the morphing process involved landmarking a template mesh with 13 anatomic and 46 additional landmarks corresponding to those used for the extracted femurs above. The template mesh comes from the right femur of the Total Human Model for Safety (THUMS) 4 (Toyota, 2011). The nodal coordinates from the template mesh, the 59 template landmark coordinates, and each patient's 59 landmark coordinates were used to determine the morphed mesh using radial basis function (RBF) morphing (Carr, 2001 and Bennink, 2006). In the second process, the morphed mesh was projected onto the surface of the patient's bone to match the patient femur geometry. Figure 1 illustrates the processes for morphing and projecting a template femur FE mesh onto extracted bone surface geometries. The morphed and projected nodal coordinates from each patient were exported for use in statistical analysis.

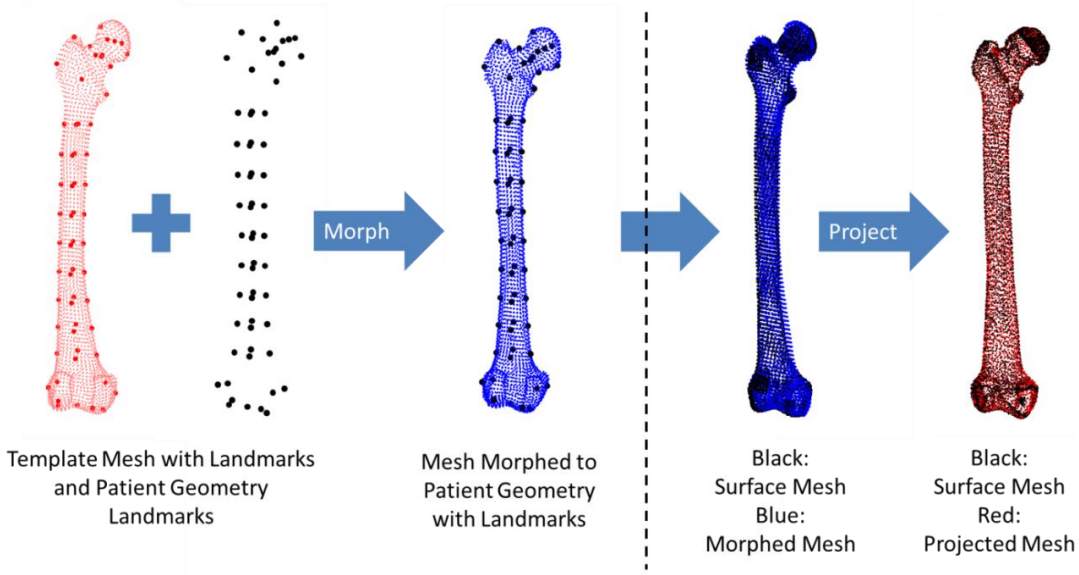

Figure 1: The morphing and projecting processes for an example femur.

Cortical Bone Thickness Calculation. The inner surfaces of cortical bone were additionally extracted from the original CT scans. An algorithm was developed in Mathematica version 8.0 (Wolfram Research, Champaign, IL) to determine cortical bone thickness along each femur using the extracted outer and inner surfaces determined by a calculated density threshold value. Lines normal to the outer surfaces were calculated at each nodal coordinate, and thickness values were determined based on distances between the outer and inner surfaces along the normal lines. The thickness values were set to a minimum value of 1.25mm if the calculated values were below the minimum resolution of the CT scans. The general outline for the cortical thickness calculation method is shown in Figure 2. The thickness values were also exported for use in the statistical analysis.

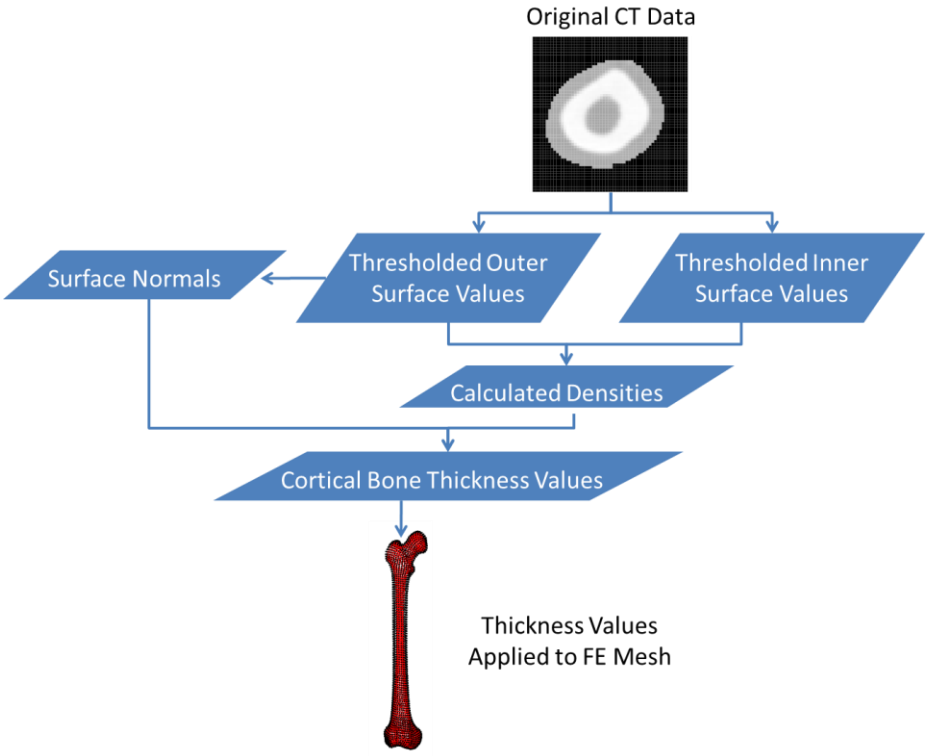

Figure 2: Outline of the cortical thickness calculation method.

Principal Component Analysis and Regression. A statistical model of the femur was developed using principal component analysis and regression (PCA+R) techniques (Reed and Parkinson, 2008 and Joliffe, 2002). The PCA method used here follows the method discussed by Li et al. (2011). First the morphed and projected coordinates were aligned using Procrustes alignment (Slice, 2007). PC scores were computed from calculating the eigenvalues and eigenvectors of the covariance matrix of a centered geometry matrix. A regression analysis was performed following the procedure used in Reed et al. (2009) to use subject parameters to predict PC scores and, in turn, to predict detailed LX geometry. Femur nodal coordinate locations and the associated cortical thickness values were predicted using this regression analysis as functions of age, BMI, and femur length (which can be predicted from stature) with separate models for male and female gender. The male and female models predicted by choosing sets of subject

characteristics, and morphing the template THUMS 4 model based on those characteristics, constitute the parametric femur FE model.

Goodness of fit was investigated to evaluate the statistical model developed for the femur. Values for cross-sectional area and cortical bone thickness along the shaft were compared between the femur data used to develop the statistical model and the femurs predicted using the original data's characteristics. The quality of the statistical analysis (linear regression) was also examined.

Material Properties. The THUMS 4 femur model uses an elasto-plastic material definition (MAT_024, MAT_PIECEWISE_LINEAR_PLASTICITY) with solid elements in LS-DYNA version 971 (Livermore Software Technology Corporation, Livermore, CA) determined from a previous validation study (Toyota 2011). A review of human bone literature revealed that the yield stress value and plastic strain to failure value used in the THUMS 4 definition did not agree with the literature, but all other material model parameters were within published ranges. The yield stress used by the THUMS model of 34.5MPa is much lower than the range of values seen in literature, i.e. approximately 100-150MPa (Burstein, 1976 and Dokko, 2009). Therefore, a material optimization was performed using modeFRONTIER version 4.3.0 (ESTECO, Italy) to determine the average yield stress (140MPa) and plastic strain to failure (0.004). All other material properties for the components in the simulations were matched to the values given in the studies used for validation.

Femur Model Validation

The femur FE model was validated by simulating tests of specific cadaver femurs in combined loading tests conducted by Ivarsson et al. (2009). The subject characteristics given in the study were used to predict specific femur bone geometry to use in the validation. An average optimized material property across subjects was used in all simulations to reasonably represent the effects of geometry without the effects of material properties on loading results. The subject characteristics for the tests used for validation are in Appendix A. Cadaver femurs from nine male and four female adult subjects were subjected to combined 3-point bending and axial compression tests. The femurs were impacted at midshaft in either the anterior to posterior or posterior to anterior direction and loaded along the long axis of the femur shaft with both the distal and proximal ends compressed toward the midshaft. The compression force was delivered by bearings connected to gussets that move when the impactor moves downward. The compression force delivered was limited by the crush strength of the honeycomb piece between the bearing and gusset on the proximal side of the femurs. All soft tissue was removed and the femurs were potted and attached to hinge joints. The simulation set-up in HyperMesh version 11.0 (Altair Engineering Inc., Troy, MI) for the combined loading is shown in Figure 3. The predicted simulation results computed in LS-DYNA were then compared to the experimentally measured test results.

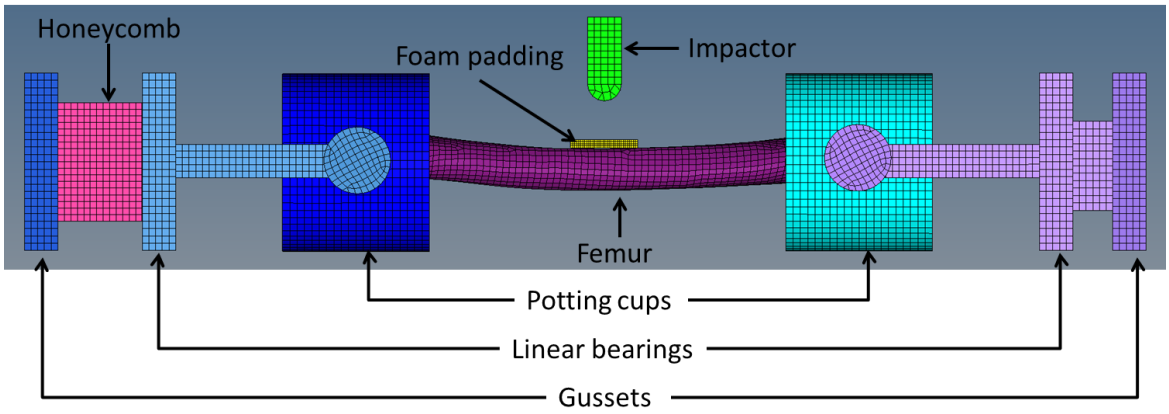

Figure 3: Ivarsson et al. test set-up with combined bending and axial compression due to the impactor and moving gussets.

Femur Model Application

Simulations were performed with scaled THUMS 4 femurs and average male and female femurs in the same 13 test set-ups performed by Ivarsson et al. to compare the parametric femur model to previous model validation methods. The THUMS 4 femur model was scaled in the x-, y-, and z-directions based on a femur length scale factor. An average material property for the scaled femurs was calculated in the same way as for the model-predicted femurs, and these values (yield stress=160MPa and plastic strain to failure=0.006) were used in the scaled femur simulations. Average male and female femurs were predicted from the average subject characteristics in the Ivarsson et al. study, and these femurs were used in the 9 male and 4 female simulations. The same average material property (yield stress=140MPa and plastic strain to failure=0.004) used for the model-predicted femurs were used for the average femurs.

A series of simulations of the Ivarsson et al. posterior-anterior compression-bending femur tests was performed to quantify the predicted effects of age, femur length, and BMI on peak impactor force. Both male and female femur geometries were predicted for a range of ages (20-80), femur lengths (predicted from 5th, 25th, 50th, 75th, and 95th percentile statures), and BMIs (15-45). The same average femur material property used for validation was also used for the tests with varying BMI and femur length to only investigate the effects of geometry. A range of material property values from a linear regression in the study by Dokko et al. were used for the tests with varying age.

RESULTS

Femur Model Development

Principal Component Analysis and Regression. Statistical models were developed in this study that can predict femur geometry for both male and female subjects as functions of age, BMI, and femur length. The femur length values can either be input directly in the statistical

models or calculated as a function of subject stature from a linear regression model. The statistical models use the same number of PC scores as number of subjects used to develop the models (36 for female and 62 for male) to include all of the variation in the data. The R^2 values for the male and female femur external geometry models are 0.968 and 0.948, and for the male and female thickness models the R^2 values are 0.219 and 0.423. The significance levels of age, BMI, and femur length on the first five PCs for the male and female external geometry and thickness models are shown in Tables 1 and 2. Femur length is the most significant parameter for the male and female external geometry models, while BMI is the most significant parameter for the male and female thickness models.

Table 1: Significance levels of parameters in the female and male external geometry models

Parameter	**p-value**				
	1st PC	2nd PC	3rd PC	4th PC	5th PC
Female Age	0.626	0.925	0.011	0.754	0.573
Female Femur Length	0.000	0.281	0.355	0.735	0.722
Female BMI	0.736	0.000	0.632	0.805	0.016
Male Age	0.434	0.000	0.040	0.809	0.190
Male Femur Length	0.000	0.427	0.710	0.550	0.859
Male BMI	0.576	0.353	0.200	0.946	0.162

Table 2: Significance levels of parameters in the female and male thickness models

Parameter	**p-value**				
	1st PC	2nd PC	3rd PC	4th PC	5th PC
Female Age	0.349	0.005	0.341	0.386	0.779
Female Femur Length	0.129	0.047	0.433	0.114	0.644
Female BMI	0.000	0.132	0.908	0.349	0.357
Male Age	0.507	0.295	0.005	0.603	0.326
Male Femur Length	0.794	0.463	0.032	0.215	0.885
Male BMI	0.000	0.308	0.158	0.336	0.331

Femurs were predicted using characteristics from the original femurs used to develop the model to ensure the model could predict the correct geometry. The average error in predicted mid-shaft cross-section cortical bone area was about 4.5% compared to the real subjects. The

cross-section areas at mid-shaft and other locations were also used to investigate the effects of occupant characteristics on area, and these distributions are in Appendix B. The errors in the thickness values were calculated to further investigate the statistical models, and the distribution in average errors along the femur shaft was investigated using box plots (Figure 4). The residuals for each model were checked for normal distributions and no trends were seen with any model parameter.

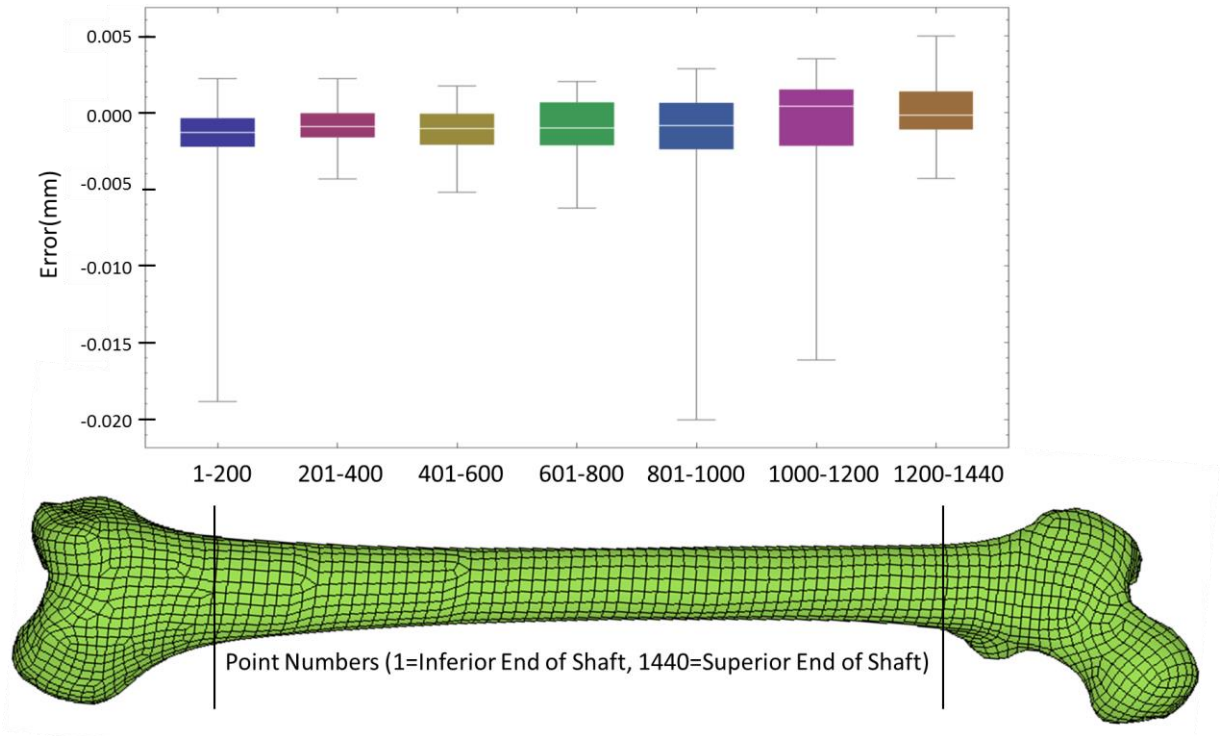

Figure 4: Ranges of the distribution of the average errors in thickness values along the femur shaft.

The parametric femur FE model generated from the statistical models consists of 3060 hexahedral elements with a total of 6124 nodes. The mesh qualities for the predicted models were close to the baseline THUMS 4 femur model. The minimum Jacobian value for the template THUMS 4 femur was 0.38, and this value was used to evaluate the mesh quality for the predicted femurs based on the Ivarsson data. Approximately 4% of all the elements for each femur fell below the 0.38 level. The majority of poor quality elements were located at the ends of the femurs (in the femoral head, neck, and condyles).

Femur Model Validation

Midshaft cross-section areas reported in the Ivarsson study were compared to those predicted by the statistical femur geometry model. The difference in cortical bone mid-shaft cross-section areas between the PMHS femurs and the model-predicted FE meshes was about 16%. The correlation between experimentally measured cross-section area and model-predicted cross-section area at mid-shaft was about 0.71 ($p=0.046$) with an R^2 value of 0.51 (Figure 5).

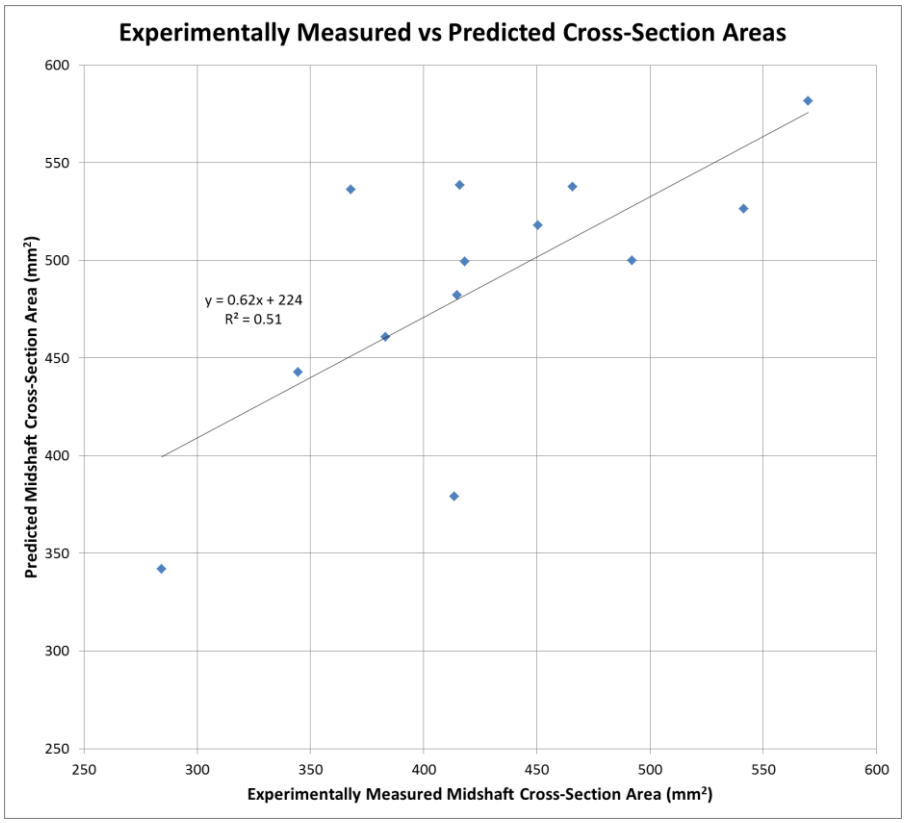

Figure 5: Correlation between experimentally measured cross-section area and predicted area at mid-shaft.

The time histories of impactor forces were compared between the experimentally measured combined loading tests and the model-predicted femur simulations. The results are in Appendix C. Peak impactor forces at the time of fracture in the tests were compared to the model-predicted impactor forces at the same time or to the fracture force if that force occurred prior to the experimentally measured time of fracture. The average percent error was 3.4% as shown in Table 3.

Femur Model Application

The simulations performed with the scaled THUMS 4 femurs and the average male and female femurs were compared to the simulations performed with the model-predicted femurs. The average error in the force curve results until fracture time was 7.6% for the scaled femurs and 3.2% for the average male and female simulations combined. The peak impactor forces at time of fracture were compared between the experimentally measured tests, the predicted femurs, the scaled femurs, and the average male and female femurs (Table 3). The predicted femurs from the parametric model had the lowest average percent error. The response curves for all of these simulations can be found in Appendix D.

Table 3: Percent differences between peak impactor forces for experimentally measured and predicted, scaled, and average male and female femur simulations at time of failure

Test ID	Gender	Peak Impactor Force (N)	Model-Predicted Peak Impactor Force (N)	Model-Predicted Percent Difference of Peak (%)	Scaled THUMS Peak Impactor Force (N)	Scaled THUMS Percent Difference of Peak (%)	Average Peak Impactor Force (N)	Average Percent Difference of Peak (%)
1.02	M	-2480	-2200	-12	-930	-63	-4500	81
1.04	M	-6880	-5610	-18	-3690	-46	-6060	-12
1.06	M	-7400	-7820	6	-5450	-26	-8430	14
1.08	M	-7470	-5940	-21	-6680	-11	-8120	9
1.09	M	-6310	-8230	31	-6120	-3	-8760	39
1.11	M	-6660	-5790	-13	-5680	-15	-6990	5
1.13	M	-9700	-8430	-13	-6450	-34	-7850	-19
1.15	M	-3580	-4660	30	-1550	-57	-4750	33
1.17	M	-6300	-7400	17	-6120	-3	-9000	43
1.19	F	-2560	-3280	28	-1090	-58	-3100	21
1.21	F	-6480	-4240	-35	-4770	-26	-6110	-6
1.23	F	-3970	-6010	51	-3100	-22	-5080	28
1.27	F	-6690	-6160	-8	-5390	-19	-6900	3
Avg:		-5890N	-5830N	3%	-4390N	-29%	-6590N	18%

Femur length, BMI, and age were varied over different ranges (with the other characteristics held constant) to investigate the effects on peak impactor force in a combined loading condition (Tables 4-6). The distributions of peak impactor force in the simulations were plotted over the varying characteristics for both male and female femur models (Figures 6-8).

Table 4: Peak impactor force before fracture in simulations with varying length

Femur Length Percentile:	**5th**	**25th**	**50th**	**75th**	**95th**
Male Peak Impactor Force (N)	-7450	-7320	-7480	-7570	-7770
Female Peak Impactor Force (N)	-5510	-5630	-5510	-5430	-5390

Table 5: Peak impactor force before fracture in simulations with varying BMI

BMI (kg/m^2):	**15**	**20**	**25**	**30**	**35**	**40**	**45**
Male Peak Impactor Force (N)	-6130	-6820	-7320	-8000	-8560	-9500	-10500
Female Peak Impactor Force (N)	-4280	-4820	-5470	-6070	-6710	-7330	-8230

Table 6: Peak impactor force before fracture in simulations with varying age

Age (years):	20	30	40	50	60	70	80
Male Peak Impactor Force (N)	-6520	-6330	-6250	-6260	-6200	-6060	-5960
Female Peak Impactor Force (N)	-4950	-4910	-4800	-4810	-4670	-4570	-4370

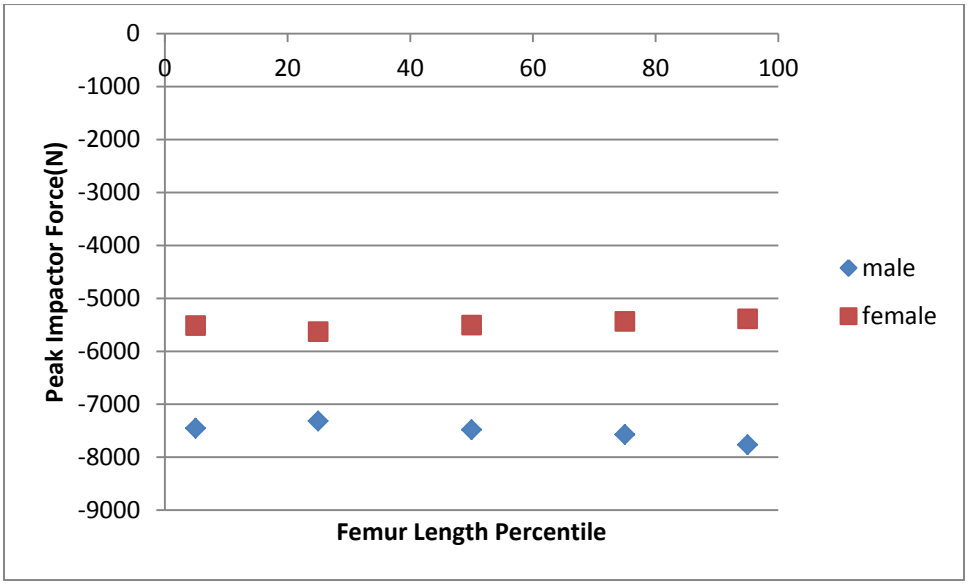

Figure 6: Distribution of peak impactor forces with varying length.

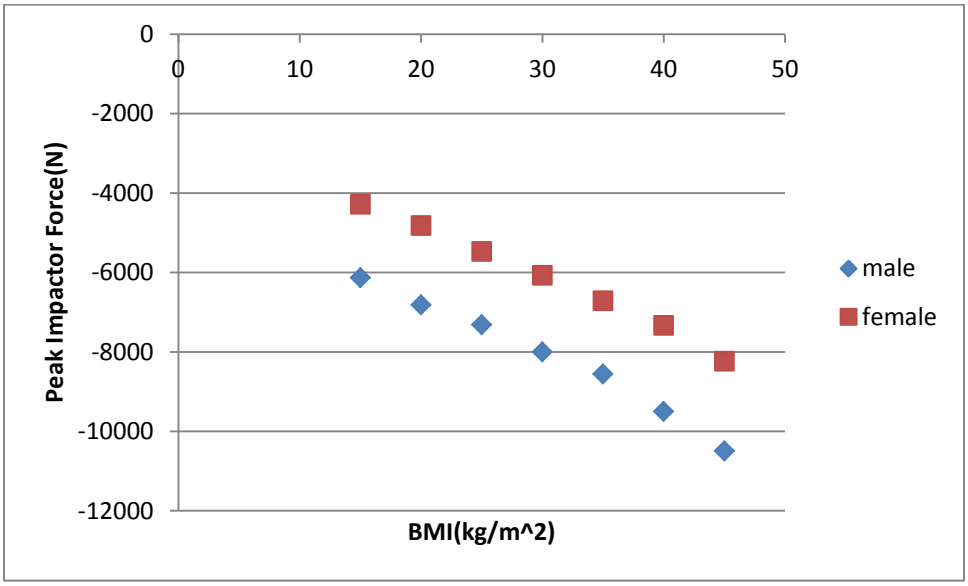

Figure 7: Distribution of peak impactor forces with varying BMI.

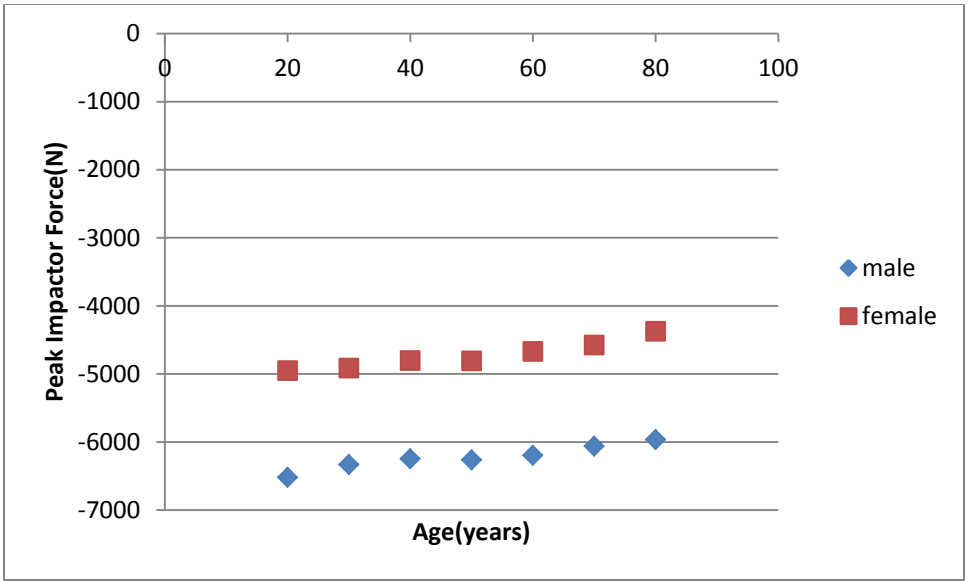

Figure 8: Distribution of peak impactor forces with varying age.

DISCUSSION

A parametric femur FE model is a useful example of the benefits for developing an entire LX parametric FE model for understanding the biomechanical factors that explain how age, gender, and BMI affect the likelihood, location, and severity of LX injuries in frontal crashes. A parametric FE femur model, LX model, and human models in general overcome the limitations in existing FE models that do not adequately account for variability in human geometry (Hu, 2012). The results shown in Table 3 indicate that a parametric model can more accurately predict human response under loading conditions than the traditional methods of scaling or using an average geometry.

Separate models were developed for external geometry and thickness, as well as male and female, to account for the different types of variation in geometry. The male and female external surface geometry models were able to predict the overall geometry with high R^2 values, but the thickness models had lower R^2 values. Overall size and shape is accounted for by the model parameters of subject age, femur length, and BMI, but thickness values can vary amongst subjects with the same set of characteristics, causing the lower R^2 values.

A limitation of this study is that only one small set of femur data was used for validation because this data set was the only known study to include all of the subject characteristics and response time histories necessary for a complete validation. This data set had a small range of subject characteristics, but some BMI values went to extreme end of the range. The over-prediction of midshaft cross-section area seen for subjects with extreme subject characteristics may be a result of the linear model being unable to predict values on the extreme ends. The over-prediction in general for the 13 subjects may be a result of differences in area calculation methods between the experimentally measured values and the predicted values.

Another limitation of this study is that an average femur material model with one set of material properties was used to account for geometry variations for the validation simulations. However, a review of human bone literature showed that femur cortical bone material properties change with age. The review also showed that femur bone geometry changes with age (bones normally increase in total diameter and marrow space normally expands with aging), leading to a larger total bone area with age but weaker bones due to the change in moment with the increase in marrow space (Clarke, 2008). Femur bones tend to get stronger with age in simulations when material properties are not varied with age due to this change in geometry. A material regression model with values related to age is included in the application section and will be included in future work to account for both geometry and material property changes with age.

The femur model developed in this study is a valuable example for developing and validating a parametric LX FE model. An entire LX model is needed to investigate the effects of age, gender, BMI, and stature on LX injuries in frontal crashes since elderly, female, and obese occupants are at increased risk for LX injury. The same methods used in this study are being used to develop parametric tibia, pelvis, and foot models. The femur, tibia, pelvis, and foot models will be combined to develop an entire LX parametric model to investigate the effects of age, gender, BMI, and stature on LX injuries in frontal crashes. The lower extremity parametric FE model can then be used as part of a whole-body FE model with parametric external surface geometry and posture morphing to eventually optimize restraint systems to better protect vulnerable populations in frontal crashes.

ACKNOWLEDGEMENT

This project was funded by the National Highway Traffic Safety Administration under contract number DTNH22-10-H-01020.

REFERENCES

BENNINK, H.E., KORBEECK, J.M., JANSSEN, B.J., ter HAAR ROMENY, B.M. (2006). Warping a Neuro-Anatomy Atlas on 3D MRI Data with Radial Basis Functions. Proc. 3rd International Conference on Biomedical Engineering, 214-218.

BURSTEIN, A.H., REILLY, D.T., MARTENS, M. (1976). Aging of Bone Tissue: Mechanical Properties. Journal of Bone and Joint Surgery, 58, 82-86.

CARR, J.C., BEATSON, R.K., CHERRIE, J.B., MITCHELL, T.J., FRIGHT, W.R., McCALLUM, B.C., EVANS, T.R. (2001). Reconstruction and Representation of 3D Objects with Radial Basis Functions. Proc. 28th Annual Conference on Computer Graphics and Interactive Techniques, 67–76.

CLARKE, B. (2008). Normal Bone Anatomy and Physiology. Clinical Journal of the American Society of Nephrology, 3, S131-S139.

DOKKO, Y., ITO, O., OHASHI, K. (2009). Development of Human Lower Limb and Pelvis FE Models for Adult and the Elderly. SAE International Paper No. 2009-01-0396.

GAYZIK, F.S., YU, M.M., DANELSON, K.A., SLICE, D.E., Stitzel, J.D. (2008). Quantification of Age-related Shape Change of the Human Rib Cage through Geometric Morphometrics. Journal of Biomechanics, 41, 1545-1554.

HU, J., RUPP, J.D., REED, M.P. (2012). Focusing on Vulnerable Populations in Crashes: Recent Advances in Finite Element Human Models for Injury Biomechanics Research, Journal of Automotive Safety and Energy, 3, 295-307.

IVARSSON, B.J., GENOVESE, D., CRANDALL, J.R., BOLTON, J.R., UNTAROIU, C.D., BOSE, D. (2009). The Tolerance of the Femoral Shaft in Combined Axial Compression and Bending Loading. Proc. 53rd Stapp Car Crash Conference, 251-290.

IWAMOTO, M., HASEGAWA, J., MIKI, K., FURUSU, K., WATANABE, I. (2002). Development of a Finite Element Model of the Total Human Model for Safety (THUMS) and Application to Injury Reconstruction. Proc. International IRCOBI Conference on the Biomechanics of Impacts.

JOLIFFE, I.T. (2002). Principal Component Analysis. 2nd ed. Springer.

KIM, Y.S., CHOI, H.H., CHO, Y.N., PARK, Y.J., LEE, J.B., YANG, K.H., KING, A.I. (2005). Numerical Investigations of Interactions between the Knee-Thigh-Hip Complex with Vehicle Interior Structures. Proc. 49th Stapp Car Crash Conference, 85-115.

KIMPARA, H., LEE, J.B., YANG, K.H., KING, A.I., IWAMOTO, M., WATANABE, I., MIKI, K. (2005). Development of a Three-Dimensional Finite Element Chest Model for the 5th Percentile Female. Proc. 49th Stapp Car Crash Conference, 251-269.

KUPPA, S., FESSAHAIE, O. (2003). An Overview of Knee-Thigh-Hip Injuries in Frontal Crashes in the United States. Proc. of the 18th International Technical Conference on the Enhances Safety of Vehicles, National Highway Traffic Safety Administration, ISSI Paper No. 416.

LI, Z., HU, J., REED, M.P., RUPP, J.D., HOFF, C.N., ZHANG, J., CHENG, B. (2011). Development, Validation, and Application of a Parametric Pediatric Head Finite Element Model for Simulations. Annals of Biomedical Engineering, 39, 2984-2997.

MORAN, S.G., McGWIN Jr, G., METZGER, J.S., ALONSO, J.E., RUE III, L.W. (2003). Relationship between Age and Lower Extremity Fractures in Frontal Motor Vehicle Collisions. Journal of Trauma, 54, 261-265.

REED, M.P., PARKINSON, M.B. (2008). Modeling Variability in Torso Shape for Chair and Seat Design. Proc. of the ASME Design Engineering Technical Conferences, Paper No. 2008-49483, 2008, 1–9.

REED, M.P., SOCHOR, M.M., RUPP, J.D., KLINICH, K.D., MANARY, M.A. (2009). Anthropometric Specification of Child Crash Dummy Pelves through Statistical Analysis of Skeletal Geometry. Journal of Biomechanics, 42, 1143–1145.

RIDELLA, S.A., BEYERSMITH, A., POLAND, K. (2011). Factors Associated with Age-Related Differences in Crash Injury Types, Causation, and Mechanisms. Available from <http://crag.uab.edu/safemobility/Presentations/2011%20TRB%20Stephen%20Ridella.pdf >.

RUAN, J.S., EL-JAWAHRI, R., BARBAT, S., ROUHANA, S.W., PRASAD, P. (2008). Impact Response and Biomechanical Analysis of the Knee-Thigh-Hip Complex in Frontal Impacts with a Full Human Body Finite Element Model. Proc. 52nd Stapp Car Crash Conference, 505-526.

RUPP, J.D. and FLANNAGAN, C.A.C. (2011). Effects of Occupant Age on AIS 3+ Injury Outcome Determined from Analyses of Fused NASS/CIREN Data. Available from < http://www.sae.org/events/gim/presentations/2011/RuppFlannagan.pdf>.

TORIGIAN, M.S. (2011). GHBMC Mid-Size Male Model 2011 Status and Future Plan. Available from <http://www.sae.org/events/gim/presentations/2011/MarkSTorigian.pdf>.

TOYOTA MOTOR CORPORATION. (2011). THUMS AM50 Pedestrian/Occupant Model Academic Version 4.0.

ROBIN, S. (2001). HUMOS: Human Model for Safety– A Joint Effort towards the Development of Refined Human-Like Car Occupants Models. Proc. 17th International Technical Conference on the Enhanced Safety of Vehicles, Paper No. 297.

SILVESTRI, C., RAY, M.H. (2009). Development of a Finite Element Model of the Knee-Thigh-Hip of a 50th Percentile Male Including Ligaments and Muscles. International Journal of Crashworthiness, 14, 215-229.

SHI, X., CAO, L., REED, M.P., RUPP, J.D., HU, J. (2014). Effects of Obesity on Occupant Responses in Frontal Crashes: A Simulation Analysis using Human Body Models. Computer Methods in Biomechanics and Biomedical Engineering, (ahead-ofprint), 1-13.

SLICE, D.E. (2007). Geometric Morphometrics. Annual Review of Anthropology, 36, 261-281.

van ROOIJ, L., van HOOF, J., McCANN, M.J., RIDELLA, S.A., RUPP, J.D., BARBIR, A., van der MADE, R., SLAATS, P. (2004). A Finite Element Lower Extremity and Pelvis

Model for Predicting Bone Injuries due to Knee Bolster Loading. SAE International Paper No. 2004-01-2130.

APPENDIX A

Table A: Subject characteristics from Ivarsson et al. (2009) data

Test ID	Age	Femur Length	BMI	Gender
1.02	51	548	492	Male
1.04	62	491	541.4	Male
1.06	62	484	450.4	Male
1.08	49	572	465.8	Male
1.09	62	501	415.9	Male
1.11	44	512	418.2	Male
1.13	58	525	569.9	Male
1.15	65	496	368	Male
1.17	53	488	414.8	Male
1.19	64	445	344.6	Female
1.21	40	430	284.2	Female
1.23	45	436	383.1	Female
1.27	50	440	413.7	Female

APPENDIX B

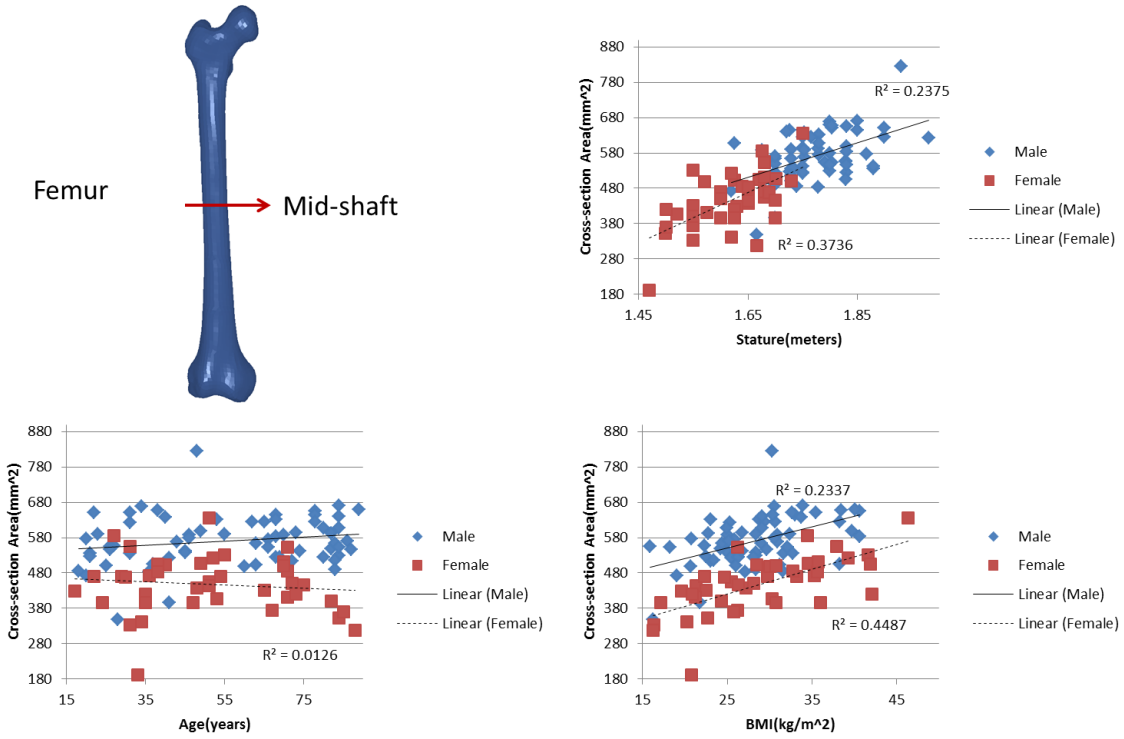

Figure B1: Effects of occupant characteristics on femur mid-shaft cross-section area for male and female subjects.

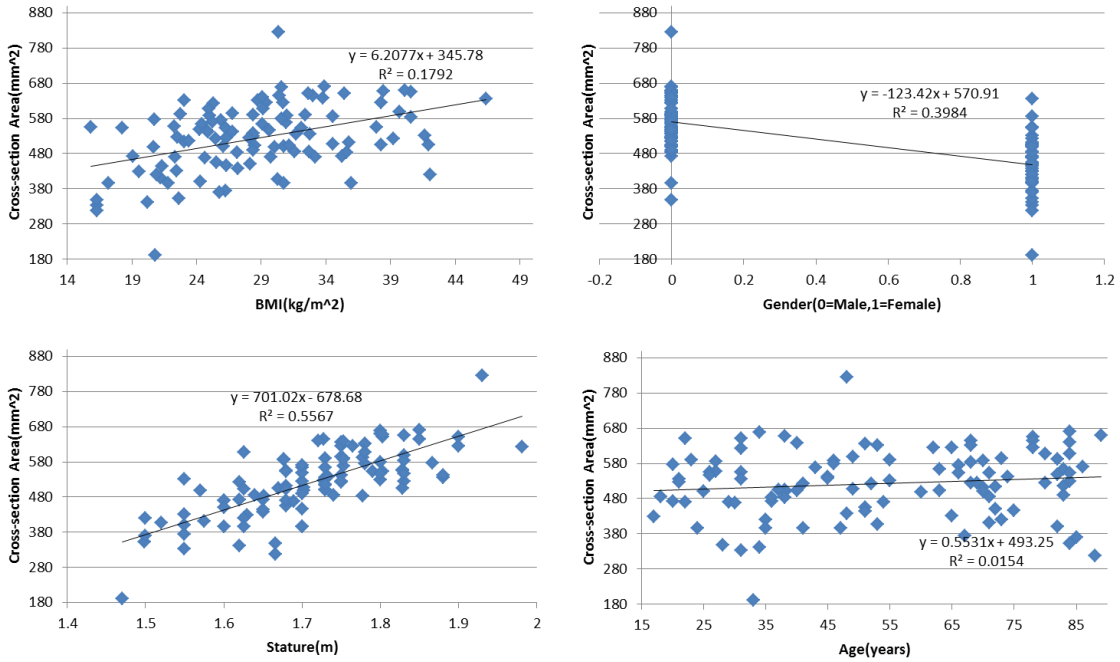

Figure B2: Effects of occupant characteristics on femur mid-shaft cross-section area for all subjects.

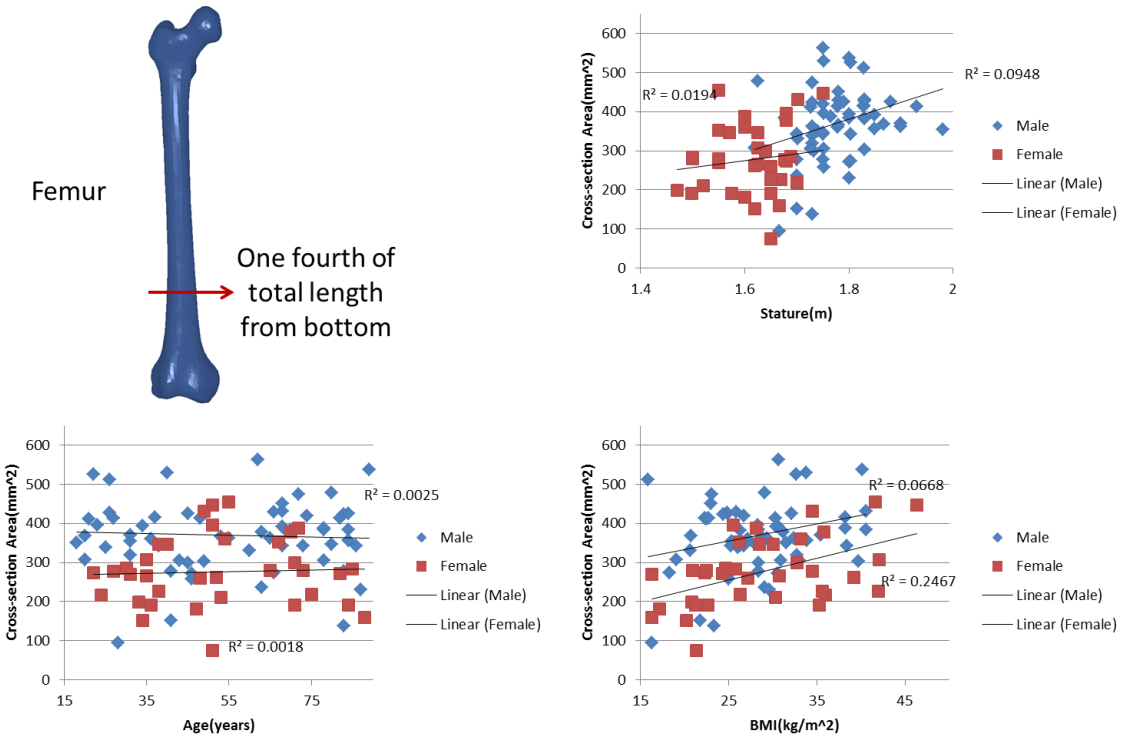

Figure B3: Effects of occupant characteristics on femur cross-section area at one fourth of total length from bottom for male and female subjects.

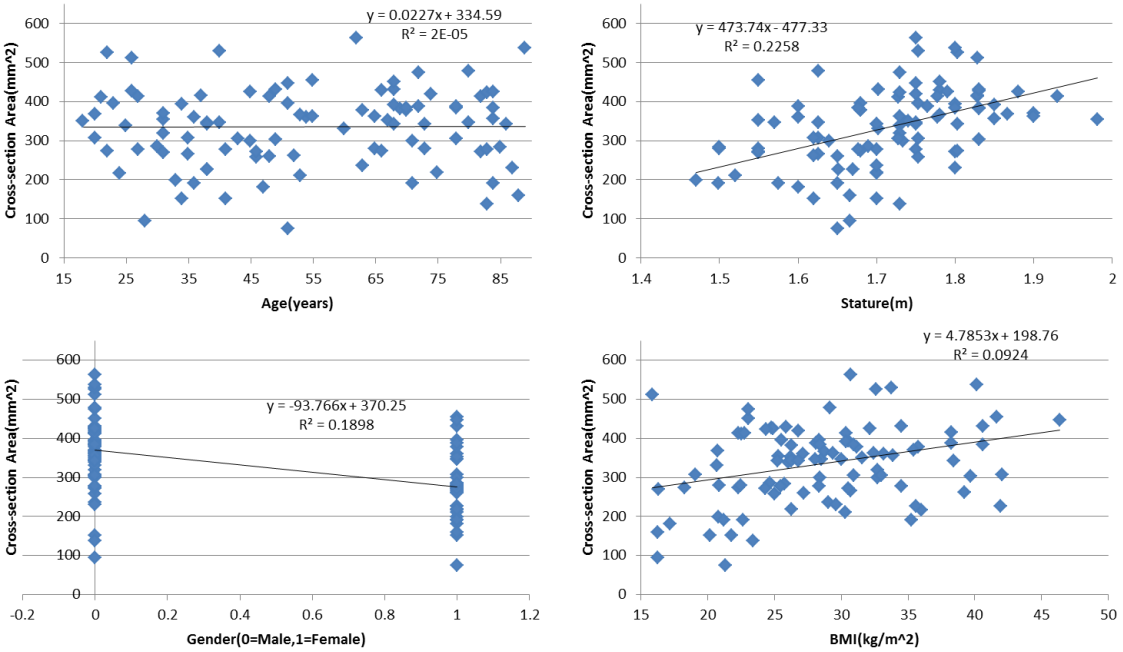

Figure B4: Effects of occupant characteristics on femur cross-section area at one fourth of total length from bottom for all subjects.

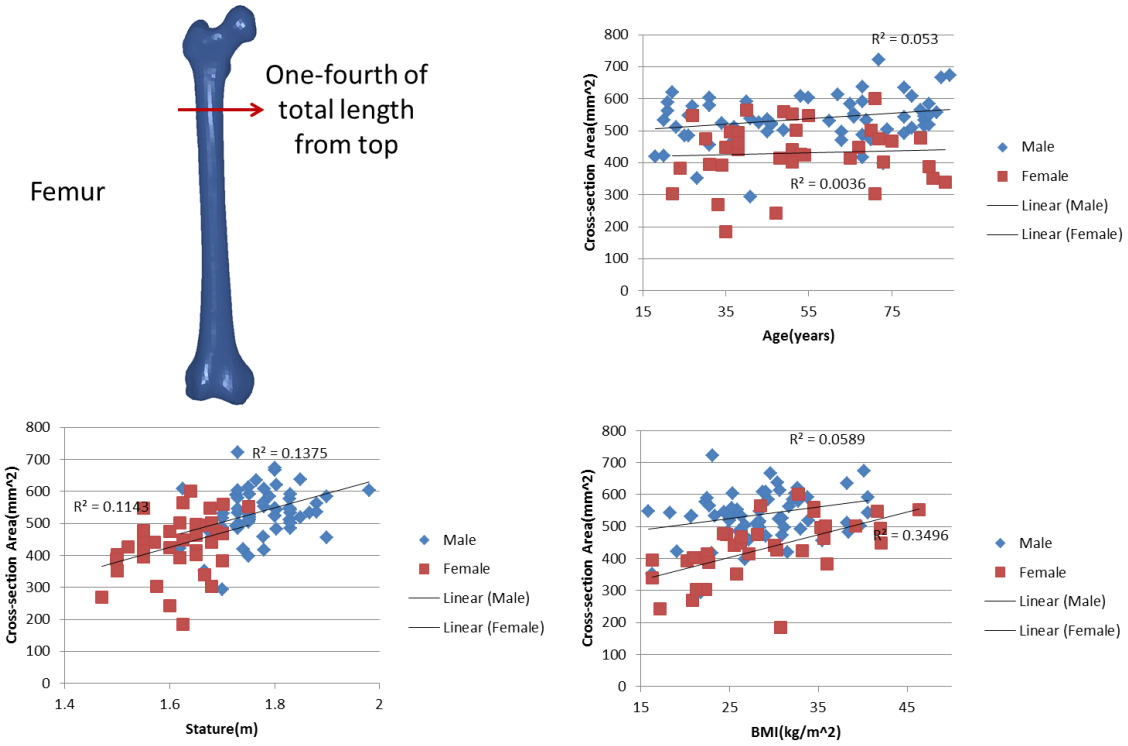

Figure B5: Effects of occupant characteristics on femur cross-section area at one fourth of total length from top for male and female subjects.

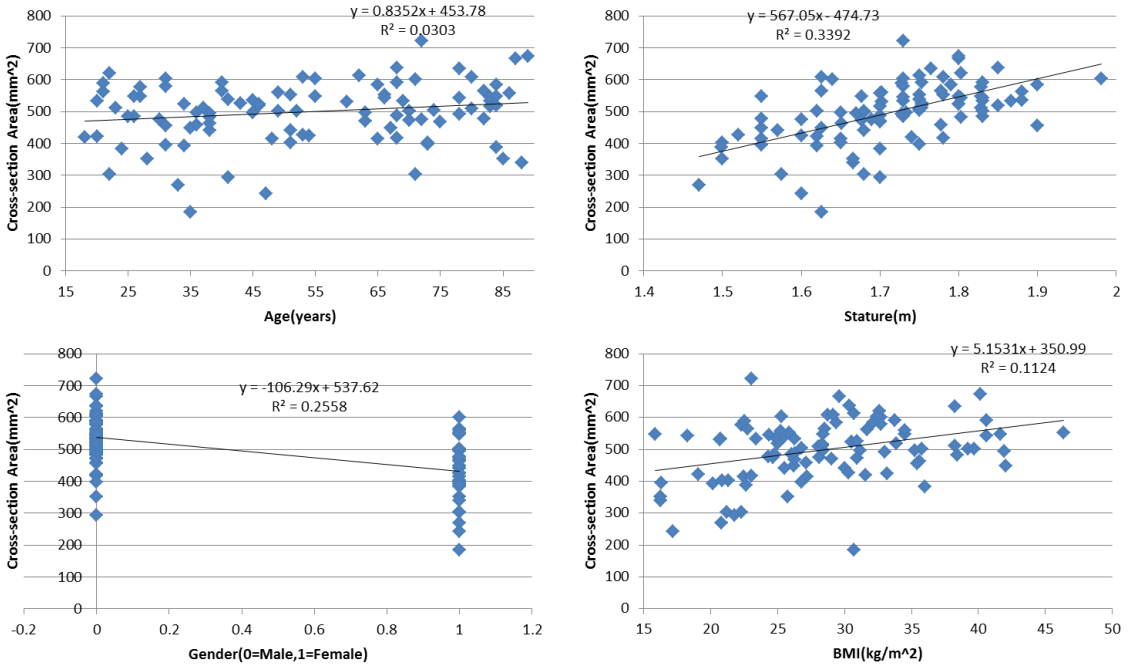

Figure B6: Effects of occupant characteristics on femur cross-section area at one fourth of total length from top for all subjects.

APPENDIX C

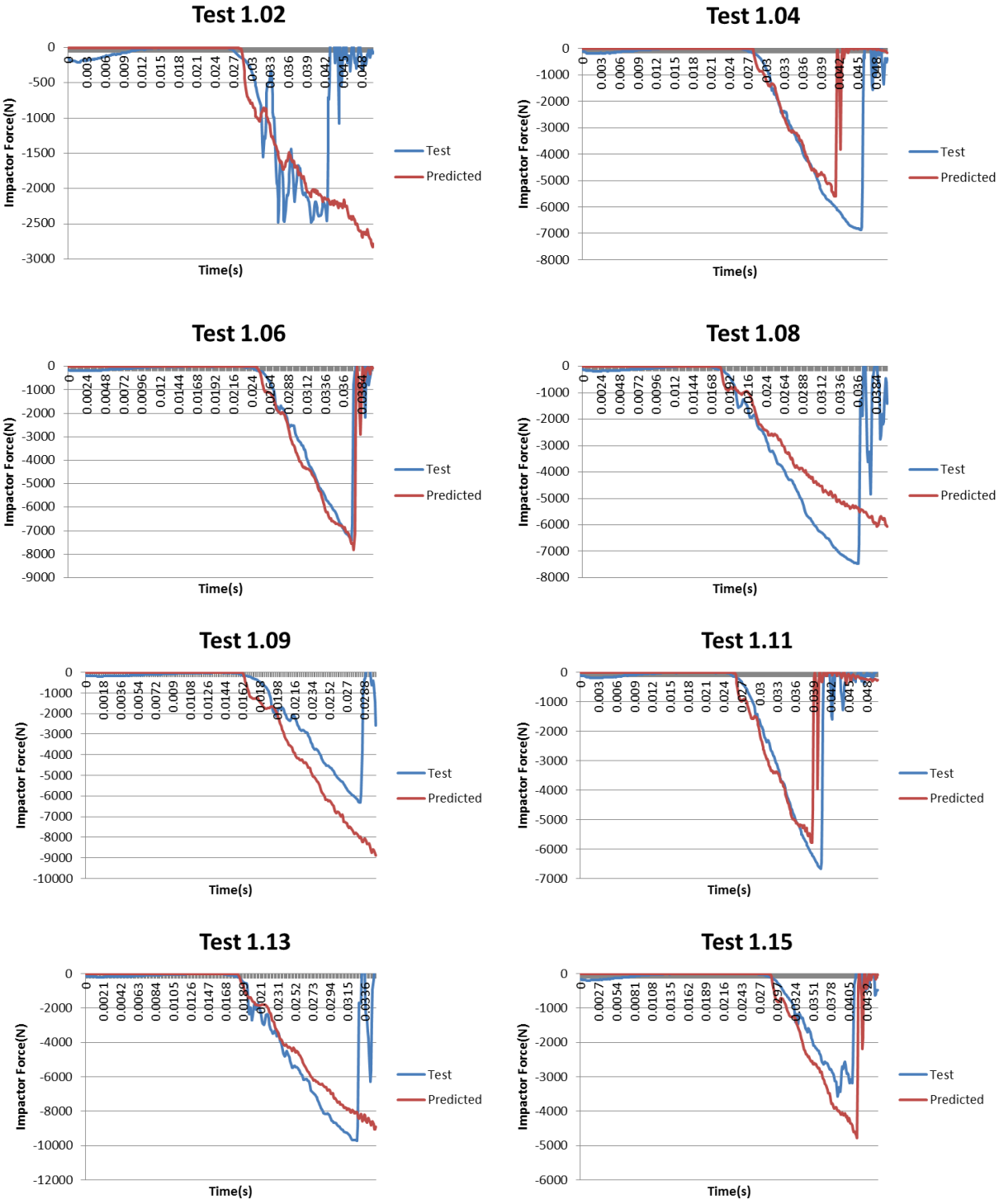
Test 1.02
Impactor Force(N)
Time(s)
Test
Predicted
Test 1.04
Impactor Force(N)
Time(s)
Test
Predicted
Test 1.06
Impactor Force(N)
Time(s)
Test
Predicted
Test 1.08
Impactor Force(N)
Time(s)
Test
Predicted
Test 1.09
Impactor Force(N)
Time(s)
Test
Predicted
Test 1.11
Impactor Force(N)
Time(s)
Test
Predicted
Test 1.13
Impactor Force(N)
Time(s)
Test
Predicted
Test 1.15
Impactor Force(N)
Time(s)
Test
Predicted

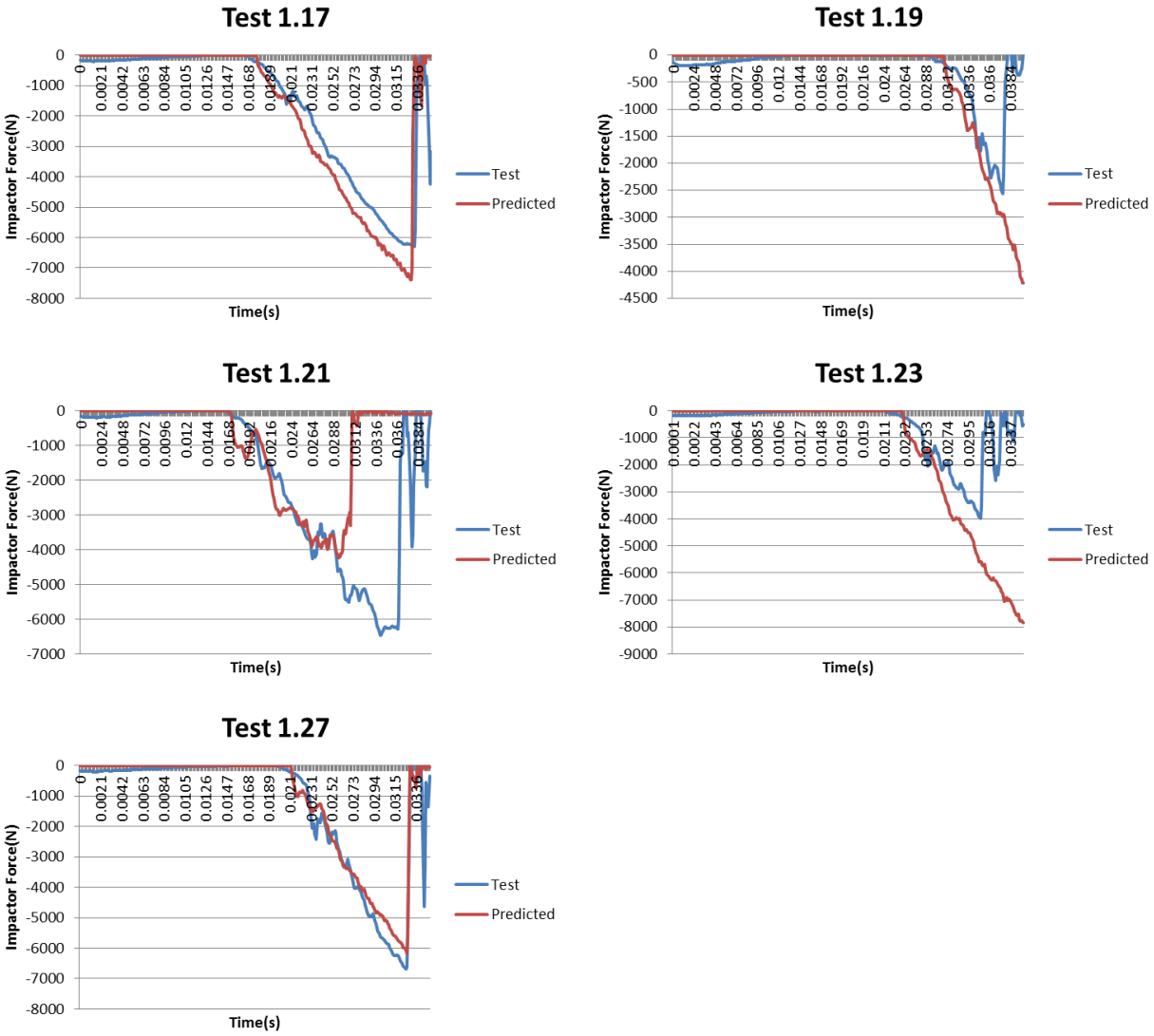

Figure C: Time histories of impactor forces for the model-predicted geometry simulations compared to the experimentally measured results.

APPENDIX D

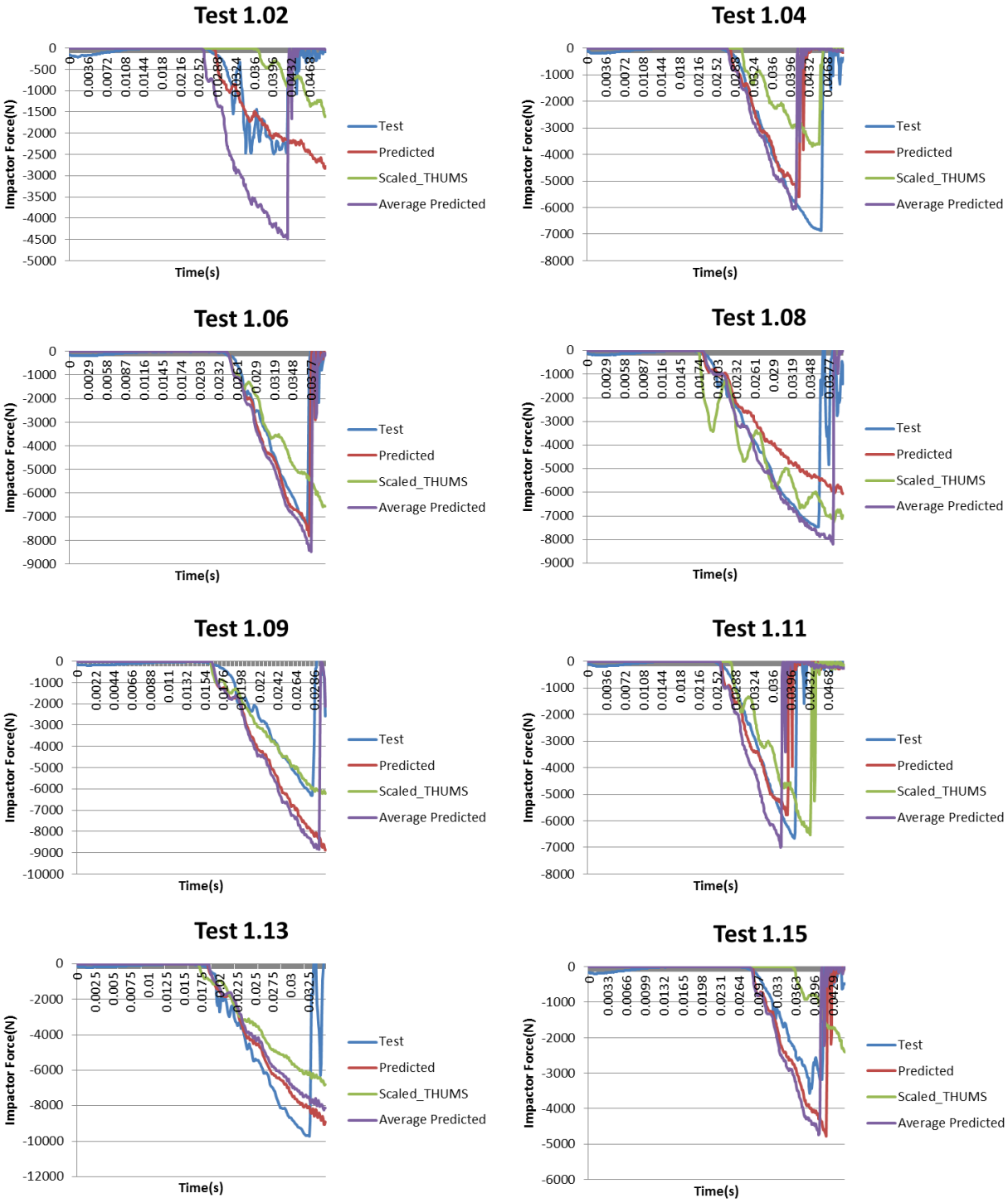
Test 1.02
Impactor Force(N)
Time(s)
Test 1.04
Test 1.06
Test 1.08
Test 1.09
Test 1.11
Test 1.13
Test 1.15
Test
Predicted
Scaled_THUMS
Average Predicted

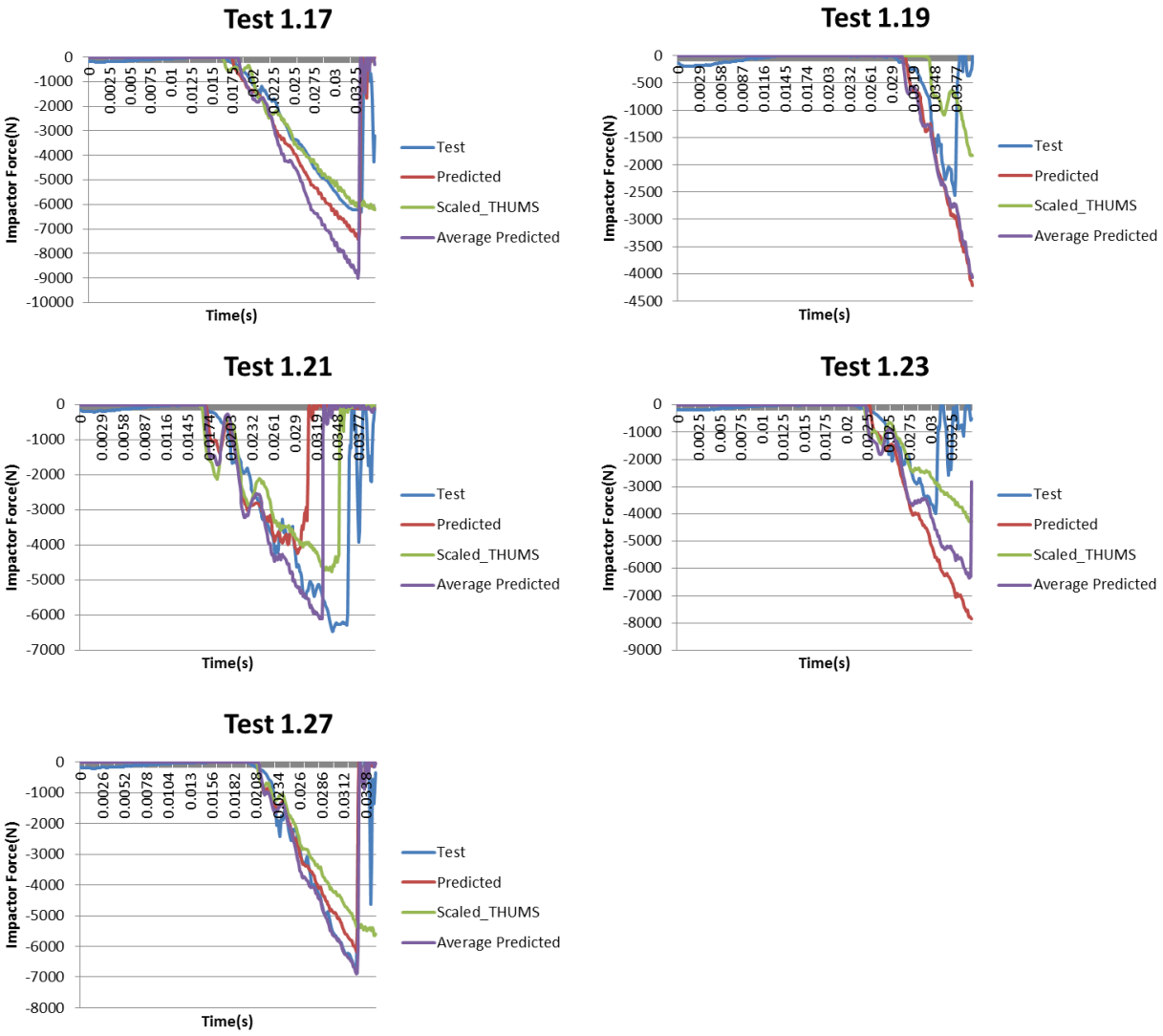

Figure D: Time histories of impactor forces for the model-predicted geometry simulations, scaled THUMS simulations, and average male and female simulations compared to the experimentally measured results.